Atmos. Chem. Phys. Discuss., doi:10.5194/acp-2016-1167, 2017
Manuscript under review for journal Atmos. Chem. Phys.
Published: 12 January 2017

Atmospheric Chemistry and Physics Discussions

Abrupt seasonal transitions in land carbon uptake in 2015

Chao Yue[1], Philippe Ciais[1], Ana Bastos[1], Frederic Chevallier[1], Yi Yin[1], Christian Rödenbeck[2]

[1]Laboratoire des Sciences du Climat et de l'Environnement, CEA-CNRS-UVSQ, UMR8212, Gif-sur-Yvette, France

[2] Max Planck Institute for Biogeochemistry, Jena, Germany.

Corresponding author: Chao Yue, chao.yue@lsce.ipsl.fr

Abstract

The year 2015 saw a record atmospheric CO_2 growth rate associated with a weaker than usual land carbon sink. Paradoxically, it was also the greenest year since 2000 according to satellite observations of vegetation greenness. To reconcile these two seemingly paradoxical observations, we examined the patterns of CO_2 fluxes using two atmospheric inversions. Inversion results indicate that the year 2015 had a higher than usual northern land carbon uptake in spring and summer, consistent with the greening anomaly. This higher uptake was however followed by a larger source of CO_2 in autumn, suggesting a coupling between growing season uptake and late season release of CO_2. For the tropics and Southern Hemisphere, a strong and abrupt transition toward a large carbon source for the last trimester of 2015 is discovered, concomitant with the El Niño development. This abrupt transition of terrestrial tropical CO_2 fluxes between two consecutive seasons is the largest ever found in the inversion records.

1 Introduction

The first monitoring station for background atmospheric CO_2 concentration was established at Mauna Loa in 1958. The record since then shows that atmospheric CO_2 continued to rise in response to anthropogenic emissions. However, the atmospheric CO_2 growth rate (AGR) has been lower than that implied by anthropogenic emissions alone, because land ecosystems and the oceans have absorbed part of the emitted CO_2 (Canadell et al., 2007; Le Quéré et al., 2016).

Atmos. Chem. Phys. Discuss., doi:10.5194/acp-2016-1167, 2017
Manuscript under review for journal Atmos. Chem. Phys.
Published: 12 January 2017

Atmospheric Chemistry and Physics Discussions

Although on multi-decadal time scale, carbon uptake by land and ocean has kept in pace with growing carbon emissions (Ballantyne et al., 2012; Li et al., 2016), large year-to-year fluctuations occur in the terrestrial carbon sink, mainly in response to climate variations induced by El Niño–Southern Oscillation (ENSO) (Wang et al., 2013, 2014) and other occasional events such as volcanic eruptions (Gu et al., 2003).

In 2015, the global monthly atmospheric CO_2 concentration surpassed 400 p.p.m. for the first time since the start of the measurements, with an unprecedented large annual growth rate of 2.96±0.09 p.p.m. yr^{-1} (https://www.esrl.noaa.gov/gmd/ccgg/trends/global.html#global_growth). This record-breaking AGR occurred simultaneously with a high value of the ENSO index (Betts et al., 2016) and the warmest land temperature on record since 1880 (https://www.ncdc.noaa.gov/cag/time-series/global/globe/land/ytd/12/1880-2015). But at the same time, 2015 was also shown to have the greenest growing season of the Northern Hemisphere since 2000 (Bastos et al., 2016). Widespread abnormally high positive anomalies of the normalized difference vegetation index (NDVI) were observed from the Terra satellite's Moderate-resolution imaging spectroradiometer (MODIS) sensor, in particular over eastern North America and large parts of Siberia. On the one hand, strong greening is expected to enhance northern land carbon uptake during the growing season; on the other hand the strong El Niño event in the second half of 2015 increased fire emissions in tropical Asia (Huijnen et al., 2016; Yin et al., 2016) and likely caused a loss of plant biomass and reduced carbon uptake, possibly associated with the prevailing high temperatures and reduced rainfall (Ahlström et al., 2015; Jiménez-Muñoz et al., 2016).

To reconcile the observed maximum global land greening with the record-high AGR in 2015, we examined land-atmosphere carbon fluxes estimated from two atmospheric inversions encompassing the last three decades and assimilating atmospheric CO_2 mole fraction records from a large number of *in situ* and flask records: the Copernicus Atmosphere Monitoring Service inversion (CAMS, version r15v3) (Chevallier et al., 2005, 2010) and the Jena CarboScope atmospheric inversion (version s04_v3.8, hereafter abbreviated as Jena04, update from Rödenbeck, 2005; Rödenbeck et al., 2003). We focus on seasonal patterns in the land carbon uptake during 2015, relative to the long-term trend of 1981-2015. We then investigate how land

Atmos. Chem. Phys. Discuss., doi:10.5194/acp-2016-1167, 2017
Manuscript under review for journal Atmos. Chem. Phys.
Published: 12 January 2017

ecosystems responded to the joint occurrences of record-breaking warming, extreme greening, and the end-of-year El Niño event, to understand how land ecosystems contributed to the high AGR in 2015.

2 Data and methods

2.1 Data sets

2.1.1 Atmospheric inversion data

We used two gridded land and ocean carbon uptake data sets based on atmospheric CO_2 observations, namely the Copernicus Atmosphere Monitoring Service (CAMS) inversion system developed at LSCE (Chevallier et al., 2005, 2010) and the Jena CarboScope inversion system developed at the MPI for Biogeochemistry Jena (update of Rödenbeck, 2005; Rödenbeck et al., 2003). Atmospheric inversions use atmospheric CO_2 concentration at observation sites, combined with an atmospheric transport model as well as prior information on carbon emissions from fossil fuel burning and on carbon exchange between the atmosphere and land (and ocean), to estimate land- and ocean-atmosphere net carbon fluxes that minimize a Bayesian cost function, which measures the mismatch between observed and simulated atmospheric CO_2 mixing ratios. Detailed information inversions could be found in respective sources as mentioned above.

The CAMS inversion data (version r15v3) were provided for 1979-2015 with a weekly time-step and a spatial resolution of 1.875° latitude and 3.75° longitude. The Jena CarboScope inversion provides daily fluxes at a spatial resolution of 3.75° latitude and 5° longitude. It offers a series of runs that use differently large station sets with complete data coverage over time, in order to avoid spurious flux variations from a changing station network. From these runs, we used s04_v3.8 (shortened as Jena04 in the main text and supplementary material) includes the largest number of measurement sites, to allow more robust constraining of carbon exchanges in 2015 (see http://www.bgc-jena.mpg.de/CarboScope/ for more details on other configurations). The s04_v3.8 run has a validity period as 2004–2015, although it does provide the data for the whole time span of 1981–2015. In the calculation of the long-term linear trend, we exceptionally use this run outside its period of validity; from a comparison of the linear trends over the latitudinal regions examined in this study between the s04_v3.8 and the long s81_v3.8 runs we established that this was possible in this case.

Atmos. Chem. Phys. Discuss., doi:10.5194/acp-2016-1167, 2017
Manuscript under review for journal Atmos. Chem. Phys.
Published: 12 January 2017

Atmospheric Chemistry and Physics Discussions

94

95 **2.2.2 Atmospheric CO_2 growth rates, NDVI and climate data**

96 Atmospheric CO_2 growth rates were retrieved from the Global Monitoring Division, Earth
97 System Research Laboratory (ESRL), NOAA
98 (http://www.esrl.noaa.gov/gmd/ccgg/trends/global.html). We used NDVI data between 2000 and
99 2015 from MODIS Terra Collection 6, re-gridded at 0.5° resolution and monthly time-step. The
100 NDVI anomalies are calculated at pixel level as the standardized monthly NDVI (i.e., de-
101 seasonalized) relative to the reference period of 2000–2014. Climate fields are from ERA interim
102 reanalysis (Dee et al., 2011) at 0.5° resolution and monthly time-step. We used air temperature,
103 precipitation and volumetric soil water content (%) integrated over the soil column to a depth of
104 2.89 m.

105

106 **2.1.3 Indices for El Niño–Southern Oscillation (ENSO) states and fire emission data**

107 We examined the seasonal variations of the carbon cycle in 2015 in relation to ENSO events and
108 compared the year 2015 with the 1997–1998 El Niño event. The Multivariate ENSO Index (MEI,
109 http://www.esrl.noaa.gov/psd/enso/mei/) was used to indicate the ENSO state. MEI is a
110 composite index calculated as the first unrotated principal component of six ENSO-relevant
111 variables for each of the twelve sliding bi-monthly seasons. The 12 bi-monthly MEI values of
112 each year are summed to obtain the annual MEI. To examine the potential role of fire emissions
113 in the land carbon balance in 2015, we used the GFED4s carbon emission data at daily time-step
114 and 0.25° spatial resolution (http://www.globalfiredata.org/data.html). Monthly fire-carbon
115 emissions were calculated for the regions and were examined for 1997–2015.

116

117 **2.2 Data analysis**

118 **2.2.1 NDVI rank analysis and greening trend**

119 First, we calculated seasonal mean standardized NDVI for each pixel and each year of the period
120 2000–2015. We examined four seasons: Q1 (January–March), Q2 (April–June), Q3 (July–
121 September) and Q4 (October–December). Given a season and a pixel, the annual time series of
122 seasonal NDVI for 2000-2015 were ranked in ascending order so that each year could be labelled
123 by a rank, with 1 being the lowest and 16 the highest rank. A spatial map of NDVI rank was then
124 obtained for each year for the given season. Vegetated area fraction with the highest rank for

Atmos. Chem. Phys. Discuss., doi:10.5194/acp-2016-1167, 2017
Manuscript under review for journal Atmos. Chem. Phys.
Published: 12 January 2017

Atmospheric Chemistry and Physics Discussions

different years was obtained, with the sum of these fractions yielding unity. This procedure was repeated for all four seasons to generate four seasonal time series, with each containing the vegetation land fractions with highest NDVI for different years. Finally, a composite map was made for year 2015, by merging pixels with the highest rank of all four seasons in 2015.

2.2.2 Analysis of 2015 land carbon uptake dynamics

Annual land and ocean carbon uptakes and carbon emissions from the two inversions were calculated for the globe over their period of overlap, 1981–2015. AGRs from NOAA/ESRL over 1981–2015 were converted into Pg C using a conversion factor of 2.12 Pg C p.p.m.$^{-1}$ (Ballantyne et al., 2012; Le Quéré et al., 2016), assuming that all the atmosphere is well mixed within one year. For comparison, land and ocean net carbon uptakes for 1981–2015 were retrieved from the Global Carbon Project (Le Quéré et al., 2016). For this purpose, a carbon flux of 0.45 Pg C yr^{-1} is subtracted from the inversion-derived land carbon uptakes and is added to ocean carbon uptakes to account for the pre-industrial land-to-ocean carbon fluxes (Jacobson et al., 2007), following Le Quéré et al. (2016).

The record high AGR in 2015 was a composite collectively determined by carbon emissions from fossil fuel burning and industry, and land and ocean carbon uptakes, all being impacted by a historical trend. Thus to properly attribute the 2015 AGR to historical trend and interannual variation, annual time series of carbon emissions, land and ocean carbon uptakes, and AGRs from NOAA/ESRL over 1981-2015 were linearly detrended to generate the detrended anomalies of AGR, emissions, and land and ocean carbon uptakes. The percentages of anomalies in carbon emissions, land and ocean sink in 2015 to the 2015 AGR anomaly were then calculated as relative contributions by each factor to the 2015 AGR anomaly.

Seasonal land carbon uptakes were also calculated (the 0.45 Pg C yr^{-1} correction was not applied). We then examined the seasonal anomalies of 2015 land carbon uptake over different regions and the globe, and the seasonal transitions. The same linear detrending was done for 1981-2015. The globe was divided into two latitude bands: Boreal and temperate Northern Hemisphere (BoTeNH, latitude > 23.5°N) and tropics and extratropical Southern Hemisphere (TroSH, latitude < 23.5°N). The BoTeNH is further divided into boreal Northern Hemisphere (BoNH, latitude > 45°N) and

Atmos. Chem. Phys. Discuss., doi:10.5194/acp-2016-1167, 2017
Manuscript under review for journal Atmos. Chem. Phys.
Published: 12 January 2017

Atmospheric Chemistry and Physics Discussions

156 temperate Northern Hemisphere (TeNH, 23.5° < latitude < 45°N) for further discussion.
157 Seasonal land carbon uptake transitions are calculated as the land sink anomaly in a given season
158 minus that of the former one. When examining transitions of land carbon uptake anomalies by
159 the CAMS inversion, we found the year 1993 has an extreme small Q3→Q4 global transition (-
160 2.85 Pg C within 6 months, < -4σ, the second lowest being the year 2015 with -1.0 Pg C) albeit
161 with a reasonable annual land carbon uptake (3.75 Pg C yr^{-1}). This is linked with an extreme high
162 Q3 and low Q4 uptake in this year, which could not be explained by any known carbon cycle
163 mechanisms. This is thus identified as a result of numerical instability of the inversion system
164 and consequently the year 1993 has been removed from all the seasonal analyses. Finally,
165 seasonal linear detrending was also performed at grid-cell level for land carbon uptakes for both
166 inversions, as well as air temperature, precipitation and soil water content.
167
168 **3 Results**
169 **3.1 Vegetation greening in 2015**
170 Figure 1a illustrates where and when higher-than-normal greenness conditions were observed in
171 different seasons of the year 2015, compared to other years of 2000–2015 (see Supplementary
172 Fig. 1 for greenness distribution for each season). On average 17% of vegetated land shows
173 record seasonal NDVI in 2015. The year with the second highest NDVI is 2014 having only 11%
174 vegetated area with record NDVI. An increase of the record-breaking NDVI occurrence over
175 time was clearly demonstrated (Fig. 1b). In short, 2015 clearly stands out as a greening outlier,
176 having the highest proportion of vegetated land being the greenest for all four seasons except for
177 the first season (despite the fact that for Q1, 2015 is still the second highest, Q1 = January to
178 March).
179
180 For Northern Hemisphere boreal and temperate regions, the seasons with highest NDVI in 2015
181 are Q2 and Q3 (Q2 = April to June; Q3 = July to September), corresponding to the growing
182 season from spring to early autumn. A pronounced greening anomaly in Q2 occurred in western
183 to central Siberia, western Canada and Alaska and eastern and southern Asia (Supplementary Fig.
184 1). Central and eastern Siberia and eastern North America showed marked greening in Q3.
185 Strong and widespread greening also occurred in the tropics during Q3 over Amazonia and the
186 savanna (or cerrado) of eastern South America, but this positive greening disappeared in Q4 (Q4

Atmos. Chem. Phys. Discuss., doi:10.5194/acp-2016-1167, 2017
Manuscript under review for journal Atmos. Chem. Phys.
Published: 12 January 2017

= October to December) especially over central to eastern Amazonia with the development of El Niño (Supplementary Fig. 1).

3.2 Global carbon balance for 1981-2015

Figure 2 shows the time series of fossil and industry carbon emissions, NOAA/ESRL AGR rates linked with ENSO climate oscillations as indicated by the Multivariate ENSO Index (MEI), and land and ocean carbon sinks for the common period of the two inversions (1981–2015) and the estimates by the Global Carbon Project (GCP). Emissions show a clear increase with time, however AGRs are more varying. The record high AGR of 2.96 p.p.m. in 2015 exceeds those in all other previous years including the extreme El Niño event in 1997–98. Interannual variability in AGR is mainly caused by land carbon sink fluctuations, with Pearson's correlation coefficients between detrended AGR and land sink < -0.8 ($p<0.01$) for both inversions (Pearson's correlation coefficient between detrended AGR and MEI being 0.27, $p<0.1$). The root mean square differences between inversion and GCP carbon sinks are 0.70 and 0.65 Pg C yr^{-1} for CAMS and Jena04 respectively for the land, and ~0.5 PgC yr^{-1} for the ocean for bother inversions, within the uncertainties of 0.8 and 0.5 Pg C yr^{-1} over 1981–2015, respectively for land and ocean as reported by GCP. The interannual variability of detrended sink anomalies for the land agrees well between inversions and GCP (with Pearson's correlation coefficient being 0.9 for both inversions, $p < 0.01$).

For 2015, the prescribed carbon emissions in the CAMS inversion are 9.9 Pg C yr^{-1}, of which 2.0 Pg C are absorbed by ocean, 1.7 Pg C by land ecosystems, with 6.2 Pg C remaining in the atmosphere, which matches the AGR from background stations of 6.3 Pg C assuming a conversion factor of 2.12 Pg C $p.p.m.^{-1}$ (Ballantyne et al., 2012; Le Quéré et al., 2016) and considering a measurement uncertainty of AGR as 0.09 p.p.m. (0.2 Pg C) for 2015. When land carbon fluxes from the inversion are linearly detrended over 1981-2015, the terrestrial sink in 2015 is 1.2 Pg C lower than normal (i.e., the trend value), but this is not an extreme value — it is only the seventh weakest sink since 1981. This weaker land uptake accounts for 82% of the positive AGR anomaly, which is 1.45 Pg C in 2015 by subtracting a linear temporal trend. Jena04 yields an AGR in 2015 that is 0.13 p.p.m. lower than the AGR based on background stations only, a difference close to the observation uncertainty. After removing the linear trends

Atmos. Chem. Phys. Discuss., doi:10.5194/acp-2016-1167, 2017
Manuscript under review for journal Atmos. Chem. Phys.
Published: 12 January 2017

over time similarly as for CAMS inversion, the land carbon uptake anomaly is -0.3 Pg C yr^{-1} in 2015 by Jena04 data, or 20% of the observed AGR anomaly, the remaining being explained by positive anomaly in fossil fuel emissions (34%), negative anomaly in ocean sink (20%), and the difference between modelled AGR and NOAA/ESRL reported AGR. Note that the land sink by GCP for 2015 is much lower than the two inversions, with detrended anomaly lower than that of CAMS, indicating even larger contribution from land to the high anomaly of AGR.

3.3 Seasonal land carbon uptake dynamics in 2015

To explain the seemingly paradox in 2015 between high greening and an only moderate terrestrial uptake, we examined seasonal land carbon flux dynamics using both inversions. The land carbon flux anomalies for each season and different regions of the globe are calculated (linearly detrended over 1981-2015), and shown in Fig. 3 (refer to Supplementary Fig. 2 for spatial distribution of flux anomalies). Positive anomalies indicate enhanced sink (or reduced source) against the linear trend (i.e., the normal state), while negative ones indicate the reverse.

At seasonal scale, both inversions indicate positive carbon uptake anomalies during Q2 and Q3 for boreal and temperate Northern Hemisphere (BoTeNH, latitude > 23.5°N), consistent with marked greening in central to eastern Siberia, eastern Europe and Canada (Fig. 1) as outlined above. However, an extreme follow-up negative (source) anomaly occurred in Q4 (Fig. 3b). These negative anomalies were lower than the 10th percentile of all anomalies in Q4 over time for both inversions and they partly cancelled the extra uptake in Q2 and Q3. As a result, on the annual time scale, the CAMS inversion shows an almost neutral land flux anomaly in BoTeNH, while the Jena04 inversion still indicates a significant positive annual anomaly.

For the tropics and extratropical Southern Hemisphere (TroSH, latitude < 23.5°N), both inversions show a weak negative land carbon anomaly for Q1 (mean value of -0.10 Pg C) in 2015, moderate anomalies in Q2 (of differing signs, with a negative one of -0.3 Pg C in CAMS and a positive one of 0.2 Pg C in Jena04). Q3 anomalies are almost carbon neutral for both inversions. In stark contrast, between Q3 and Q4, both inversions show an abrupt shift toward an abnormally big land carbon source (i.e., negative anomalies of ~ -0.7 Pg C against a carbon source expected from the linear trend, lower than 10th percentile over time in both inversions).

Atmos. Chem. Phys. Discuss., doi:10.5194/acp-2016-1167, 2017
Manuscript under review for journal Atmos. Chem. Phys.
Published: 12 January 2017

Atmospheric Chemistry and Physics Discussions

On the annual time scale, CAMS shows a large negative anomaly of -1.2 Pg C. For Jena04, sink and source effects in Q1–Q3 cancelled each other, leaving the annual anomaly the same as in Q4.

Over the globe, the Jena04 inversion shows an abnormally strong sink during Q2 (normal state being a net carbon sink), owing to synergy of enhanced Q2 uptakes in both BoTeNH and TroSH. This abnormally enhanced uptake partly counteracted the strong shift toward source in Q4 (normal state being a net carbon source), leaving a small negative annual land carbon balance of -0.3 Pg C. For the CAMS inversion, because of the co-occurrence of enhanced carbon release in BoTeNH and the sudden shift toward a large carbon source in TroSH both in Q4 (normal states being both net carbon sources), the land shows a strong global shift toward being a source in Q4, leaving a negative annual carbon anomaly of -1.2 Pg C (i.e., carbon sink being reduced compared with the normal state).

These consistent results from both inversions point to very strong seasonal shifts in the land carbon balance as an emerging feature of 2015. We thus calculated ***transitions*** in land carbon uptake anomaly as the first-order difference in flux anomalies between two consecutive seasons (defined as the anomaly in a given season minus that in the former one) for all years of the period 1982-2015 (Fig. 4). The ranks of transitions for different seasons relative to other years between the two inversions are broadly similar, except for Q1→Q2 and Q2→Q3 in TroSH, mainly due to the differences between the two inversions in seasonal land-carbon uptake anomaly in Q2 (Fig. 3b). On the global scale, both inversions show an extreme transition to a negative uptake anomaly for Q3→Q4, with 2015 being the largest transition of the period 1982-2015 (a transition towards an enhanced carbon source of -1.0 Pg C in 6 months). The abnormal transitions for Q3→Q4 on the global scale are located in the TroSH region, where both inversions show that during 1982-2015 the largest transition occurred in 2015. For BoTeNH, both inversions showed strong transitions toward positive anomaly for Q1→Q2; however, the same strong transition toward source anomaly occurred in Q3→Q4, partly cancelling the sink effects during growing seasons.

4 Discussion

4.1 Seasonal land carbon uptake transitions in northern latitudes

Atmos. Chem. Phys. Discuss., doi:10.5194/acp-2016-1167, 2017
Manuscript under review for journal Atmos. Chem. Phys.
Published: 12 January 2017

The two inversions consistently allocate a strong positive carbon uptake anomaly in the BoTeNH during spring, which persists through summer (Q2–Q3): an extreme sink anomaly is simulated in Q2 by Jena04, but a more moderate one by CAMS (still above the 75th percentile). The strong sink in Q2 simulated by CAMS is dominated by temperate Northern Hemisphere regions (TeNH, 23.5° < latitude < 45°N, Supplementary Fig. 3). For Q3, an extreme carbon sink anomaly occurs in boreal Northern Hemisphere (BoNH, latitude > 45°N) in CAMS; however, an equally strong negative anomaly (i.e., reduced sink) was found in TeNH in the same season, leaving the whole boreal and temperate Northern Hemisphere (BoTeNH) only a moderate enhanced sink anomaly. Thus for TeNH alone, CAMS indicates extreme seasonal shift from a positive anomaly in Q2 to a negative one in Q3, implying abrupt seasonal transitions probably resulting from enhanced ecosystem CO_2 release after growing-season uptake.

Jena04 inversion agrees with a higher-than-normal sink in TeNH (23.5° < latitude < 45°N) during spring (Q2). It also reports a moderate positive anomaly for Q3 in BoNH, but does not show a strong negative anomaly (i.e., reduced sink) in TeNH in Q3 as CAMS does. This is possibly related to differences in the measurement station data used, to different land prior fluxes (from the ORCHIDEE model in CAMS, and the LPJ model in Jena CarboScope), or to the fact that Jena inversion has a larger a-priori spatial error correlation length scale for its land fluxes (1275 km) than CAMS (500 km) (Chevallier et al., 2010; Rödenbeck et al., 2003). Nonetheless, both inversions consistently indicate that the enhancement of CO_2 uptake during spring and summer at the northern hemispheric scale was subsequently offset by an extreme source anomaly in autumn (Q4).

The transition from carbon sink anomalies during Q2 and Q3 in the Northern Hemisphere to a source anomaly during Q4 could be related with prevailing high temperatures in Q4, especially over most of northern America, and central to eastern Siberia and Europe (Supplementary Fig. 4a). The strong source anomaly in temperate regions during summer (Q3) as indicated by CAMS may also be partly due to the extreme drought that affected Europe (Supplementary Fig. 4b, see also Orth et al., 2016) and led to vegetation browning (decreased NDVI) in this region (Bastos et al., 2016). The transition toward carbon source in Q4, albeit strong uptake and high greening during the preceding seasons (especially in southern to eastern Asia in Q4), highlights the

Atmos. Chem. Phys. Discuss., doi:10.5194/acp-2016-1167, 2017
Manuscript under review for journal Atmos. Chem. Phys.
Published: 12 January 2017

311 importance of carbon release in the autumn (Piao et al., 2008) and the carry-over effect of higher
312 leaf and fine root biomass produced in spring and summer being decomposed a few months later
313 at the end of the year.
314
315 **4.2 Seasonal land carbon uptake transitions in tropics and influences of El Niño and**
316 **vegetation fire**
317 The abrupt transition to abnormal source in the tropics and extratropical Southern Hemisphere
318 was paralleled by a marked decrease in precipitation and an increase in temperature in Q4, with
319 the development of El Niño in Q2–Q3 (Supplementary Fig. 5). Here El Niño development is
320 indicated by the rise of the MEI. This abrupt transition is consistent with the expected response
321 of tropical and sub-tropical southern ecosystems during previous El Niño events (Ahlström et al.,
322 2015; Cox et al., 2013; Poulter et al., 2014; Wang et al., 2013, 2014).
323
324 Compared with the 1997–98 El Niño, which was of similarly extreme magnitude, the 2015 El
325 Niño started much earlier with positive MEI appearing during the first half of 2014. Since then
326 until Q3 and Q4 in 2015 when El Niño began to reach its peak, the tropics and Southern
327 Hemisphere saw continuous higher-than-normal temperatures, with continually decreasing
328 precipitation and accumulating deficit in soil water content (Supplementary Fig. 5). From Q3 to
329 Q4, a steep decline is further observed in both precipitation and soil moisture with stagnating
330 high temperature anomaly, which is probably a major cause of the abrupt shift toward carbon
331 source anomaly. The CAMS inversion shows a carbon source anomaly in Q4 of 2015 slightly
332 smaller than that in Q3 of 1997, while the Jena04 inversions shows almost equal magnitudes of
333 loss in land sink strength between these two extreme El Niño events. On the one hand, El Niño in
334 late 2015 started with an early onset and built upon the cumulative effects of the drought since
335 the beginning of the year; it thus came with larger negative anomaly in precipitation and soil
336 water content than the 1997–98 El Niño. This sequence of events might favour a stronger land
337 carbon source. On the other hand, the fire emission anomaly in the tropics in 2015 was less than
338 half of that in 1997 at the peak of El Niño (Fig. S5), which might contribute to a smaller land
339 source anomaly in 2015 than in 1997–98.
340
341 El Niño events are usually associated with increased vegetation fires, and these have a large

Atmos. Chem. Phys. Discuss., doi:10.5194/acp-2016-1167, 2017
Manuscript under review for journal Atmos. Chem. Phys.
Published: 12 January 2017

342 impact on the global carbon cycle (van der Werf et al., 2004). Global fire emissions of carbon
343 reached 3.0 and 2.9 Pg C in 1997 and 1998 according to the GFED4s data. These two years
344 produced the largest source of fire-emitted carbon for the entire period 1997–2015. Global fire
345 emissions in 2015 reached 2.3 Pg C, close to the 1997-2015 average (2.2 Pg C yr^{-1}) but 23–24%
346 lower than 1997–98 — the difference mainly occurring in the southern tropics (0–23.5°S, Fig.
347 S5). In particular, carbon emissions from deforestation and peat fires were two times lower in
348 2015 (0.6 Pg C) compared with 1997 (1.2 Pg C) (GFED4s data), and emissions for these types of
349 fires are more likely to be a net source contribution, because they cannot be compensated by
350 vegetation regrowth within a short time. Fire emission data thus suggest a smaller contribution
351 from fires to AGR in 2015 than 1997–98. If both annual time series of AGR and global fire-
352 carbon emissions are detrended within their overlapping period of 1997-2015, fire-carbon
353 emissions have an anomaly of 0.4 Pg C yr^{-1} in 2015, explaining only 29% of the AGR anomaly.
354
355 **4.3 Data uncertainties and perspective**
356 On the global and hemispheric scales, the inversion-derived land- and ocean-atmosphere fluxes
357 are well constrained by the observed atmospheric CO_2 growth rates on measurement sites.
358 However, because the observational network is heterogeneous and sites are sparsely distributed
359 (Supplementary Fig. 6), land CO_2 fluxes cannot be resolved precisely over each grid cell
360 (Kaminski et al., 2001) and some regions are better constrained than others. This could hinder
361 the precise matching between gridded CO_2 flux maps and climate states or the occurrence of
362 climate extremes; consequently, exact attribution of carbon uptake transitions into different
363 climate drivers could be elusive. Further, a few other uncertainties matter for the specific
364 objective of this study. First, the atmospheric network increased over time, so that the inversions
365 have a better ability to detect and quantify a sharp transition in CO_2 fluxes occurring in the last
366 than in the first decade of the period analysed. This might hide the detection of other more
367 extreme end-of-year carbon transitions during early years of our target period (1981-2015).
368 Second, because measurements for the early 2016 are not used in the CAMS inversion and not
369 completely available in the Jena inversion, the constraining of last season in 2015 is weaker than
370 for the other three seasons. This could partly influence the exact magnitude of the extreme Q4
371 negative anomaly in land carbon uptake reported here. Third, the sparse sites located in the
372 boreal Eurasia and tropical regions might diminish the ability of inversion systems to robustly

Atmos. Chem. Phys. Discuss., doi:10.5194/acp-2016-1167, 2017
Manuscript under review for journal Atmos. Chem. Phys.
Published: 12 January 2017

allocation carbon fluxes spatially, which could yield high uncertainty in the carbon fluxes diagnosed for these regions (van der Laan-Luijkx et al., 2015; Stephens et al., 2007).

Despite these uncertainties, the abrupt transition of CO_2 fluxes analysed here is the largest ever found in the inversion records. While transition to a strong source in TroSH is congruent with the expected response of ecosystems to the peak of an El Niño event, it is not completely clear which mechanisms are driving the reported abrupt seasonal transitions on the global scale. For instance, for the tropics and Southern Hemisphere, it is unclear whether the dry conditions already in place before the full development of El Niño implied moderate Q2 and Q3 vegetation carbon uptakes followed by moderate respiration as well in Q4, or if it is mainly due to enhanced respiration in late 2015 that dominated such a transition. For the boreal and temperate Northern Hemisphere, further investigation is still needed to verify whether a coupling between strong spring/summer uptake and autumn release is something intrinsic to natural ecosystems, or if strong transitions to autumn release are triggered by abrupt climate shifts. This could be evaluated by process-based and data-driven models to partition the overall sink anomaly into individual responses of photosynthesis and respiration, but that is beyond the scope of this work. Our results point to the need to better understand the drivers of carbon dynamics at seasonal, or even shorter time scales at the regional to global level, especially the link between such dynamics and climate extremes. Such understanding would help better predictions of the response of the carbon cycle to multiple long-term drivers such as atmospheric CO_2 growth and climate change.

5 Conclusions

We investigated seasonal dynamics of land carbon uptake in 2015 using data from two atmospheric inversions, focusing on reconciling the seemingly paradox between the greatest vegetation greenness and the highest atmospheric CO_2 growth rate. We found that lands in Northern Hemisphere started with a higher-than-normal sink for the northern growing seasons, consistent with enhanced vegetation greenness partly owing to elevated warming, however this enhanced sink was partly balanced by enhanced carbon release in autumn and winter. For tropics and Southern Hemisphere, a strong and abrupt transition toward a large carbon source for the last quarter of 2015 was found, concomitant with the peak of El Niño development. This abrupt transition of terrestrial CO2 fluxes in the last quarter is the largest in the inversion records since

Atmos. Chem. Phys. Discuss., doi:10.5194/acp-2016-1167, 2017
Manuscript under review for journal Atmos. Chem. Phys.
Published: 12 January 2017

Atmospheric Chemistry and Physics Discussions

1981. The abrupt transitions in CO_2 fluxes diagnosed in this study form an interesting test bed for evaluating ecosystem models and gaining understanding of their controlling processes.

Atmos. Chem. Phys. Discuss., doi:10.5194/acp-2016-1167, 2017
Manuscript under review for journal Atmos. Chem. Phys.
Published: 12 January 2017

Atmospheric Chemistry and Physics Discussions

References

Ahlström, A., Raupach, M. R., Schurgers, G., Smith, B., Arneth, A., Jung, M., Reichstein, M., Canadell, J. G., Friedlingstein, P., Jain, A. K., Kato, E., Poulter, B., Sitch, S., Stocker, B. D., Viovy, N., Wang, Y. P., Wiltshire, A., Zaehle, S. and Zeng, N.: The dominant role of semi-arid ecosystems in the trend and variability of the land CO2 sink, Science, 348(6237), 895–899, doi:10.1126/science.aaa1668, 2015.

Ballantyne, A. P., Alden, C. B., Miller, J. B., Tans, P. P. and White, J. W. C.: Increase in observed net carbon dioxide uptake by land and oceans during the past 50 years, Nature, 488(7409), 70–72, doi:10.1038/nature11299, 2012.

Bastos, A.m Ciais, P., Park, T., Zscheischler, J., Yue, C., Barichivich, J., Myneni, R.B., Peng, S.S., Piao, S.L., Zhu Z. Was the extreme Northern Hemisphere greening in 2015 predictable? Submitted to Environ. Res. Lett.

Canadell, J. G., Le Quéré, C., Raupach, M. R., Field, C. B., Buitenhuis, E. T., Ciais, P., Conway, T. J., Gillett, N. P., Houghton, R. A. and Marland, G.: Contributions to accelerating atmospheric CO2 growth from economic activity, carbon intensity, and efficiency of natural sinks, Proc. Natl. Acad. Sci., 104(47), 18866–18870, 2007.

Chevallier, F., Fisher, M., Peylin, P., Serrar, S., Bousquet, P., Bréon, F.-M., Chédin, A. and Ciais, P.: Inferring CO2 sources and sinks from satellite observations: Method and application to TOVS data, J. Geophys. Res. Atmospheres, 110(D24), D24309, doi:10.1029/2005JD006390, 2005.

Chevallier, F., Ciais, P., Conway, T. J., Aalto, T., Anderson, B. E., Bousquet, P., Brunke, E. G., Ciattaglia, L., Esaki, Y., Fröhlich, M., Gomez, A., Gomez-Pelaez, A. J., Haszpra, L., Krummel, P. B., Langenfelds, R. L., Leuenberger, M., Machida, T., Maignan, F., Matsueda, H., Morguí, J. A., Mukai, H., Nakazawa, T., Peylin, P., Ramonet, M., Rivier, L., Sawa, Y., Schmidt, M., Steele, L. P., Vay, S. A., Vermeulen, A. T., Wofsy, S. and Worthy, D.: CO2 surface fluxes at grid point scale estimated from a global 21 year reanalysis of atmospheric measurements, J. Geophys. Res. Atmospheres, 115(D21), D21307, doi:10.1029/2010JD013887, 2010.

Cox, P. M., Pearson, D., Booth, B. B., Friedlingstein, P., Huntingford, C., Jones, C. D. and Luke, C. M.: Sensitivity of tropical carbon to climate change constrained by carbon dioxide variability, Nature, 494(7437), 341–344, doi:10.1038/nature11882, 2013.

Dee, D. P., Uppala, S. M., Simmons, A. J., Berrisford, P., Poli, P., Kobayashi, S., Andrae, U., Balmaseda, M. A., Balsamo, G., Bauer, P., Bechtold, P., Beljaars, A. C. M., van de Berg, L., Bidlot, J., Bormann, N., Delsol, C., Dragani, R., Fuentes, M., Geer, A. J., Haimberger, L., Healy, S. B., Hersbach, H., Hólm, E. V., Isaksen, L., Kållberg, P., Köhler, M., Matricardi, M., McNally, A. P., Monge-Sanz, B. M., Morcrette, J.-J., Park, B.-K., Peubey, C., de Rosnay, P., Tavolato, C., Thépaut, J.-N. and Vitart, F.: The ERA-Interim reanalysis: configuration and performance of the data assimilation system, Q. J. R. Meteorol. Soc., 137(656), 553–597, doi:10.1002/qj.828, 2011.

Gu, L., Baldocchi, D. D., Wofsy, S. C., Munger, J. W., Michalsky, J. J., Urbanski, S. P. and Boden, T. A.: Response of a Deciduous Forest to the Mount Pinatubo Eruption: Enhanced Photosynthesis, Science, 299(5615), 2035–2038, doi:10.1126/science.1078366, 2003.

Huijnen, V., Wooster, M. J., Kaiser, J. W., Gaveau, D. L. A., Flemming, J., Parrington, M., Inness, A., Murdiyarso, D., Main, B. and Weele, M. van: Fire carbon emissions over maritime southeast Asia in 2015 largest since 1997, Sci. Rep., 6, 26886, doi:10.1038/srep26886, 2016.

447 Jacobson, A. R., Mikaloff Fletcher, S. E., Gruber, N., Sarmiento, J. L. and Gloor, M.: A joint atmosphere-
448 ocean inversion for surface fluxes of carbon dioxide: 1. Methods and global-scale fluxes, Glob.
449 Biogeochem. Cycles, 21(1), GB1019, doi:10.1029/2005GB002556, 2007.

450 Jiménez-Muñoz, J. C., Mattar, C., Barichivich, J., Santamaría-Artigas, A., Takahashi, K., Malhi, Y.,
451 Sobrino, J. A. and Schrier, G. van der: Record-breaking warming and extreme drought in the Amazon
452 rainforest during the course of El Niño 2015–2016, Sci. Rep., 6, 33130, doi:10.1038/srep33130, 2016.

453 Kaminski, T., Rayner, P. J., Heimann, M. and Enting, I. G.: On aggregation errors in atmospheric
454 transport inversions, J. Geophys. Res. Atmospheres, 106(D5), 4703–4715, doi:10.1029/2000JD900581,
455 2001.

456 van der Laan-Luijkx, I. T., van der Velde, I. R., Krol, M. C., Gatti, L. V., Domingues, L. G., Correia, C.
457 S. C., Miller, J. B., Gloor, M., van Leeuwen, T. T., Kaiser, J. W., Wiedinmyer, C., Basu, S., Clerbaux, C.
458 and Peters, W.: Response of the Amazon carbon balance to the 2010 drought derived with CarbonTracker
459 South America, Glob. Biogeochem. Cycles, 29(7), 2014GB005082, doi:10.1002/2014GB005082, 2015.

460 Li, W., Ciais, P., Wang, Y., Peng, S., Broquet, G., Ballantyne, A. P., Canadell, J. G., Cooper, L.,
461 Friedlingstein, P., Le Quéré, C., Myneni, R. B., Peters, G. P., Piao, S. and Pongratz, J.: Reducing
462 uncertainties in decadal variability of the global carbon budget with multiple datasets, Proc. Natl. Acad.
463 Sci., 113(46), 13104–13108, doi:10.1073/pnas.1603956113, 2016.

464 Orth, R., Zscheischler, J. and Seneviratne, S. I.: Record dry summer in 2015 challenges precipitation
465 projections in Central Europe, Sci. Rep., 6, 28334, doi:10.1038/srep28334, 2016.

466 Piao, S., Ciais, P., Friedlingstein, P., Peylin, P., Reichstein, M., Luyssaert, S., Margolis, H., Fang, J., Barr,
467 A., Chen, A., Grelle, A., Hollinger, D. Y., Laurila, T., Lindroth, A., Richardson, A. D. and Vesala, T.: Net
468 carbon dioxide losses of northern ecosystems in response to autumn warming, Nature, 451(7174), 49–52,
469 doi:10.1038/nature06444, 2008.

470 Poulter, B., Frank, D., Ciais, P., Myneni, R. B., Andela, N., Bi, J., Broquet, G., Canadell, J. G.,
471 Chevallier, F., Liu, Y. Y., Running, S. W., Sitch, S. and van der Werf, G. R.: Contribution of semi-arid
472 ecosystems to interannual variability of the global carbon cycle, Nature, 509(7502), 600–603,
473 doi:10.1038/nature13376, 2014.

474 Le Quéré, C., Andrew, R. M., Canadell, J. G., Sitch, S., Korsbakken, J. I., Peters, G. P., Manning, A. C.,
475 Boden, T. A., Tans, P. P., Houghton, R. A., Keeling, R. F., Alin, S., Andrews, O. D., Anthoni, P.,
476 Barbero, L., Bopp, L., Chevallier, F., Chini, L. P., Ciais, P., Currie, K., Delire, C., Doney, S. C.,
477 Friedlingstein, P., Gkritzalis, T., Harris, I., Hauck, J., Haverd, V., Hoppema, M., Klein Goldewijk, K.,
478 Jain, A. K., Kato, E., Körtzinger, A., Landschützer, P., Lefèvre, N., Lenton, A., Lienert, S., Lombardozzi,
479 D., Melton, J. R., Metzl, N., Millero, F., Monteiro, P. M. S., Munro, D. R., Nabel, J. E. M. S., Nakaoka,
480 S., O'Brien, K., Olsen, A., Omar, A. M., Ono, T., Pierrot, D., Poulter, B., Rödenbeck, C., Salisbury, J.,
481 Schuster, U., Schwinger, J., Séférian, R., Skjelvan, I., Stocker, B. D., Sutton, A. J., Takahashi, T., Tian,
482 H., Tilbrook, B., Laan-Luijkx, I. T. van der, Werf, G. R. van der, Viovy, N., Walker, A. P., Wiltshire, A.
483 J. and Zaehle, S.: Global Carbon Budget 2016, Earth Syst. Sci. Data, 8(2), 605–649, doi:10.5194/essd-8-
484 605-2016, 2016.

485 Rödenbeck, C.: Estimating CO2 sources and sinks from atmospheric mixing ratio measurements using a
486 global inversion of atmospheric transport, Max Planck Institute for Biogeochemistry., 2005.

487 Rödenbeck, C., Houweling, S., Gloor, M. and Heimann, M.: CO2 flux history 1982–2001 inferred from

488 atmospheric data using a global inversion of atmospheric transport, Atmos Chem Phys, 3(6), 1919–1964,
489 doi:10.5194/acp-3-1919-2003, 2003.

490 Stephens, B. B., Gurney, K. R., Tans, P. P., Sweeney, C., Peters, W., Bruhwiler, L., Ciais, P., Ramonet,
491 M., Bousquet, P., Nakazawa, T., Aoki, S., Machida, T., Inoue, G., Vinnichenko, N., Lloyd, J., Jordan, A.,
492 Heimann, M., Shibistova, O., Langenfelds, R. L., Steele, L. P., Francey, R. J. and Denning, A. S.: Weak
493 Northern and Strong Tropical Land Carbon Uptake from Vertical Profiles of Atmospheric CO2, Science,
494 316(5832), 1732–1735, doi:10.1126/science.1137004, 2007.

495 Wang, W., Ciais, P., Nemani, R. R., Canadell, J. G., Piao, S., Sitch, S., White, M. A., Hashimoto, H.,
496 Milesi, C. and Myneni, R. B.: Variations in atmospheric CO2 growth rates coupled with tropical
497 temperature, Proc. Natl. Acad. Sci., 110(32), 13061–13066, doi:10.1073/pnas.1219683110, 2013.

498 Wang, X., Piao, S., Ciais, P., Friedlingstein, P., Myneni, R. B., Cox, P., Heimann, M., Miller, J., Peng, S.,
499 Wang, T., Yang, H. and Chen, A.: A two-fold increase of carbon cycle sensitivity to tropical temperature
500 variations, Nature, 506(7487), 212–215, doi:10.1038/nature12915, 2014.

501 van der Werf, G. R., Randerson, J. T., Collatz, G. J., Giglio, L., Kasibhatla, P. S., Arellano, A. F., Olsen,
502 S. C. and Kasischke, E. S.: Continental-Scale Partitioning of Fire Emissions During the 1997 to 2001 El
503 Niño/La Niña Period, Science, 303(5654), 73–76, doi:10.1126/science.1090753, 2004.

504 Yin, Y., Ciais, P., Chevallier, F., van der Werf, G. R., Fanin, T., Broquet, G., Boesch, H., Cozic, A.,
505 Hauglustaine, D., Szopa, S. and Wang, Y.: Variability of fire carbon emissions in equatorial Asia and its
506 nonlinear sensitivity to El Niño, Geophys. Res. Lett., 2016GL070971, doi:10.1002/2016GL070971, 2016.

507

508 **Acknowledgements**

509 We thank Taejin Park from Department of Earth and Environment, Boston University for
510 making the NDVI data available. C.Y. and P.C. acknowledge funding from the European
511 Commission's 7th Framework Programme, under grant agreement number 603542 (LUC4C).
512 The work of F.C. was funded by the Copernicus Atmosphere Monitoring Service, implemented
513 by the European Centre for Medium-Range Weather Forecasts (ECMWF) on behalf of the
514 European Commission. We thank all the scientists involved in the surface and aircraft
515 measurement of atmospheric CO_2 concentration and in archiving these data and making them
516 available.

517

518 **Author contributions**

519 P.C., F.C., C.Y. and A.B. conceived the study. C.Y. performed the analysis and made the first
520 draft. F.C. and C.R. provided the inversion data. All authors contributed to interpretation of the
521 results and drafting the paper.

Atmos. Chem. Phys. Discuss., doi:10.5194/acp-2016-1167, 2017
Manuscript under review for journal Atmos. Chem. Phys.
Published: 12 January 2017

Atmospheric Chemistry and Physics Discussions

522 **Figure 1 Year 2015 as the greenest year over the period 2000-2015**. **(a)** Distribution of
523 seasons for which 2015 NDVI ranks the highest during the period 2000-2015. Yellow-coloured
524 pixels indicate grid cells where 2015 NDVI ranks highest for more than one season. For each
525 season, the fraction of global vegetated land area for which 2015 NDVI ranks highest is shown
526 in the inset colour bar. **(b)** Temporal evolution of the percentage of vegetated land with highest
527 NDVI over 2000-2015 for each season and different years. The sum total of vertical-axis values
528 for each season over all years is 100%. Q1 = January–March; Q2 = April–June; Q3 = July–
529 August; Q4 = September–December.

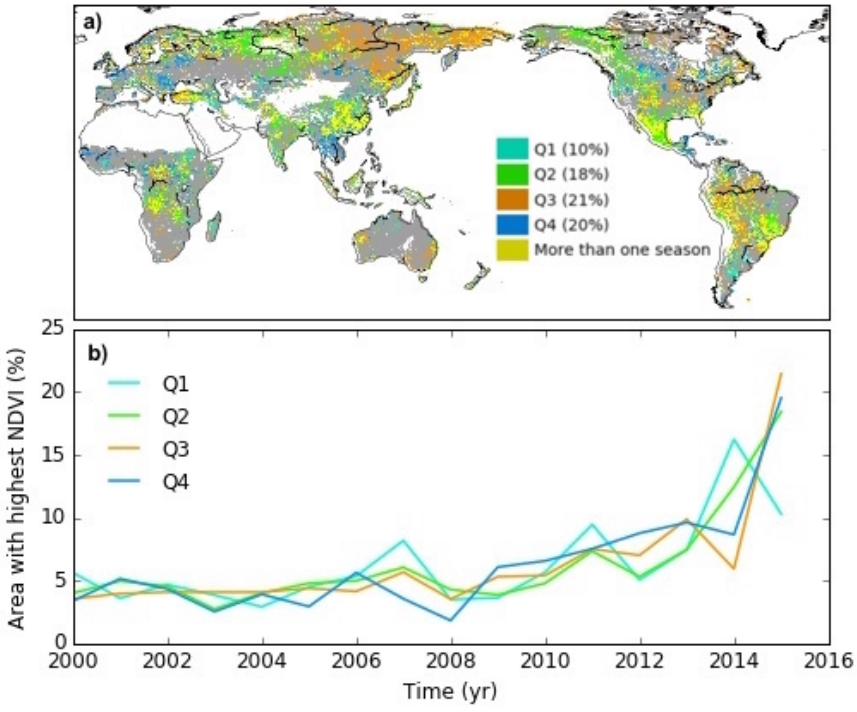

530

Atmos. Chem. Phys. Discuss., doi:10.5194/acp-2016-1167, 2017
Manuscript under review for journal Atmos. Chem. Phys.
Published: 12 January 2017

Atmospheric Chemistry and Physics Discussions

Figure 2 Global carbon fluxes and atmospheric CO_2 growth rates for 1981–2015. (a) Carbon emissions from fossil fuel and industry used in the CAMS (blue) and Jena04 (orange) inversions, **(b)** annual atmospheric CO_2 growth rate (AGR, in red) from NOAA/ESRL linked with Multivariate ENSO Index (in purple), and **(c)** land and **(d)** ocean carbon sinks for 1981-2015. Emissions and land and ocean carbon sinks from the Global Carbon Project (GCP, in black) are also shown for comparison. In subplots c and d, a carbon flux of 0.45 Pg C yr^{-1} was used to correct inversion-derived land and ocean sinks to account for pre-industrial land-to-ocean carbon flux as in Le Quéré et al. (2016). All numbers indicate values in 2015 (Pg C yr^{-1}), with those in brackets showing linearly detrended anomalies for the same year.

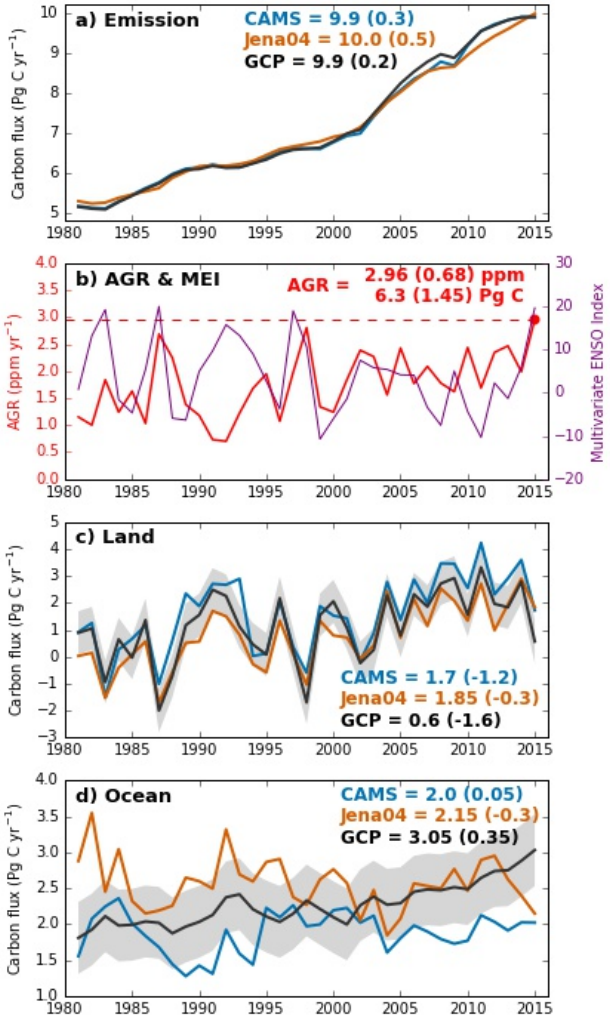

Atmos. Chem. Phys. Discuss., doi:10.5194/acp-2016-1167, 2017
Manuscript under review for journal Atmos. Chem. Phys.
Published: 12 January 2017

Atmospheric Chemistry and Physics Discussions

Figure 3 Seasonal land carbon uptake anomalies in 2015. Data are linearly detrended over 1981-2015 for different seasons in 2015, by CAMS (blue) and Jena04 (orange) inversion data. Open or solid dots indicate seasonal values (Pg C seasaon^{-1}) and vertical bars indicate annual sum (Pg C yr^{-1}). Data are shown for: **(a)** boreal and temperate Northern Hemisphere (BoTeNH, > 23.5°N), **(b)** tropics and southern extratropical hemisphere (TroSH, < 23.5°N) and **(c)** the whole globe. Solid dots indicate seasonal land carbon uptake anomalies below 10th or above 90th percentiles over 1981-2015.

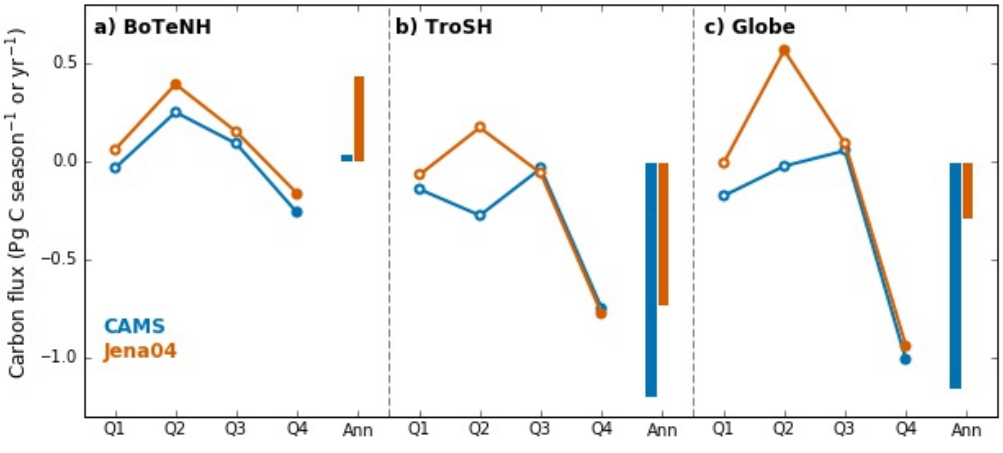

Atmos. Chem. Phys. Discuss., doi:10.5194/acp-2016-1167, 2017
Manuscript under review for journal Atmos. Chem. Phys.
Published: 12 January 2017

Atmospheric Chemistry and Physics Discussions

549 **Figure 4 Extremeness of transitions in seasonal land carbon uptake anomaly in 2015.**
550 Histograms for seasonal land carbon uptake transitions over 1981-2015 for boreal and temperate
551 Northern Hemisphere (BoTeNH, latitude > 23.5°N), tropics and extratropical Southern
552 Hemisphere (TroSH, latitude < 23.5°N) and the whole globe. Transition between two
553 consecutive seasons is defined as the linearly detrended land carbon uptake anomaly in a given
554 season minus that in the former one. Coloured bars show histograms for CAMS data (red colour
555 for a negative transition and green colour for a positive one), with the vertical-axis indicating
556 frequency and blue solid vertical line indicating year 2015. Grey step lines indicate histograms
557 for Jena04 data overlaid on top of CAMS data, with vertical orange solid lines indicating values
558 for 2015.

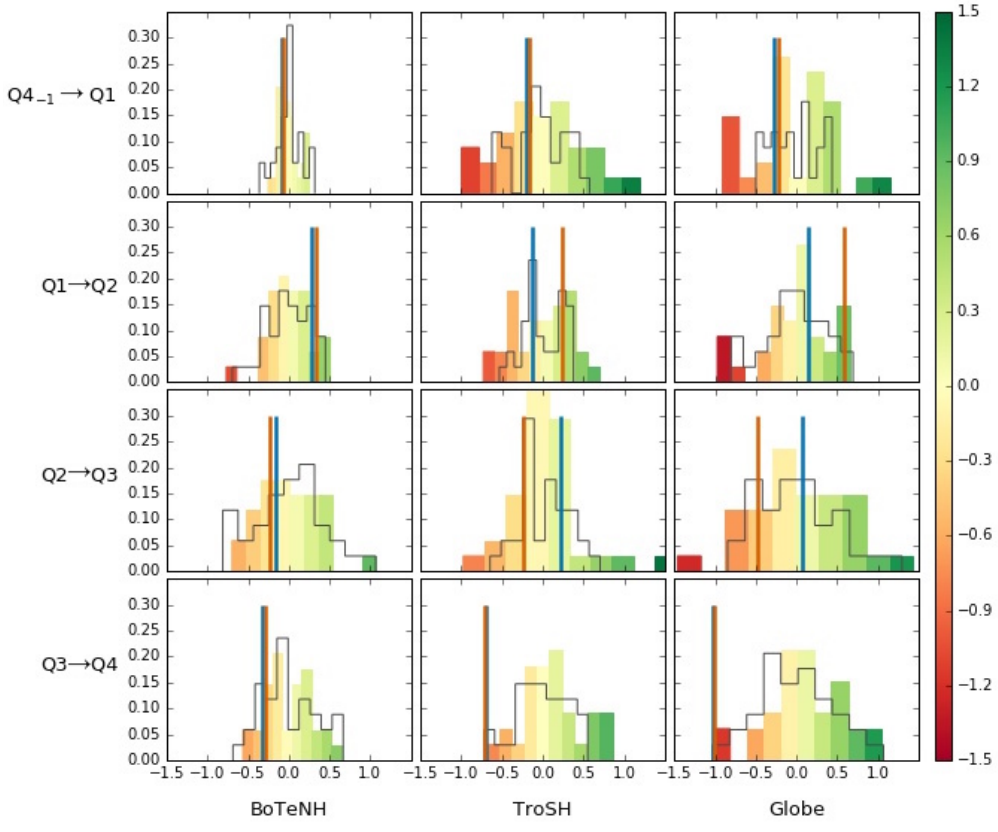

559